Vibrational Spectroscopy 118 (2022) 103328

Contents lists available at ScienceDirect

Vibrational Spectroscopy

journal homepage: www.elsevier.com/locate/vibspec

Micro-Raman mapping of VO_2 (T) microcrystals orientation

Petr Shvets [a,*], Alexander Shabanov [b], Ksenia Maksimova [a], Alexander Goikhman [a]

[a] Research and Educational Center "Functional Nanomaterials", Immanuel Kant Baltic Federal University, Aleksandra Nevskogo 14, 236041, Kaliningrad, Russian Federation

[b] Kirensky Institute of Physics FRC «KSC of SB RAS», Academgorodok str. 50/12, Krasnoyarsk, 660036, Russian Federation

ARTICLE INFO

Keywords:
Thin films
VO_2 polymorphs
VO_2 (T)
Raman scattering
Electron backscatter diffraction

ABSTRACT

Microcrystals orientation distribution in triclinic vanadium dioxide VO_2 (T) films was investigated by polarized Raman scattering with a resolution of few μm and confirmed by electron backscatter diffraction. Euler angles used to describe the orientation of the crystal were determined by two different techniques and good agreement between the values was achieved. Finally, it was demonstrated that Raman scattering could be used to identify the direction of the lattice vector ***c*** for (002) crystals in consequence of the triclinic nature of VO_2 (T).

1. Introduction

Raman spectroscopy is routinely used to analyze the phase composition of unknown samples, including biological molecules, [1] carbon materials [2], minerals [3,4], oxides [5,6], gases [7] and others. Every molecule or crystal has its own set of vibrations or phonon modes and their energies and relative intensities directly obtained in Raman spectrometer provide easy identification of the sample structure. Unfortunately, simulating Raman spectra requires complex DFT calculations and usually it is not possible to predict phonon energies for a sample with known structure accurately due to limitations of existing theories [8–10]. Thus the database of experimental reference spectra is required. Besides simple structural identification, Raman spectra may be used to determine different physical or chemical properties of the sample. Simple equations or correlation curves may be derived to find the dependence of Raman line positions, widths or relative intensities on the sample temperature [11,12], stress [13,14], chemical composition [15–17], lengths or orders of chemical bonds [18], size of crystals [19].

Raman spectrometers are usually equipped with linearly polarized lasers. Interaction of polarized light with anisotropic media depends on the orientation of the polarization vector. For single crystal samples, this leads to the significant dependence of relative Raman peak intensities on sample orientation. [20,21], This dependence can be described in terms of Raman tensor R [22]: $I \sim \boldsymbol{e_i} R \boldsymbol{e_s}$, where I is the Raman intensity and $\boldsymbol{e_i}$ and $\boldsymbol{e_s}$ are the unit polarization vectors of the incident and scattered laser beams, respectively. R depends on crystal orientation as $R = \Phi(\varphi,\theta,\psi) R_{cr} \Phi^{-1}(\varphi,\theta,\psi)$, where Φ is the transformation matrix of Euler's angles (φ, θ, ψ) required to bring the crystal into coincidence with principal axes directions and R_{cr} is a Raman tensor expressed in this axes directions (Φ^{-1} corresponds to the inverse matrix of Φ). If crystal orientation is known (angles φ and θ) and a set of measurements including in-plane crystal rotation is done (dependence of Raman mode intensity I on Euler angle ψ), one can determine Raman tensor elements R_{cr}. It has recently been done for some important materials including $BaTiO_3$ [23], $CrPS_4$ [24], black phosphorus, [25,26], SnSe [27], graphene [28], AlN [29], VO_2 (M1) [30] and many biological systems [31]. Similarly, if Raman tensor R_{cr} is known and $I(\psi)$ is measured, it is possible to determine the orientation of the crystal. The most advanced systems can do this automatically yielding an accuracy better than 1 °. [32] An important advantage of this technique is the capability to build full three-dimensional orientation maps of the grains.

Vanadium dioxide (VO_2) demonstrates sharp near room temperature metal-insulator transition from an insulating monoclinic low-temperature M1 phase to a conductive tetragonal high-temperature R phase. [33] The mechanism of this transition is debatable [34] and may involve the formation of intermediate phases such as triclinic VO_2 (T). [35] Recently, we produced a VO_2 (T) film with micrometer-sized single crystal domains and used polarized Raman scattering measurements to determine tensor elements for this phase. [36] In this work, we use values of these elements to build orientational maps of VO_2 (T) microcrystalline film. We also build similar maps applying the conventional technique for it, electron backscatter diffraction, and compare the results.

* Corresponding author.
E-mail address: pshvets@kantiana.ru (P. Shvets).

https://doi.org/10.1016/j.vibspec.2021.103328
Received 13 September 2021; Received in revised form 24 November 2021; Accepted 26 November 2021
Available online 29 November 2021

2. Material and methods

Vanadium dioxide films were deposited by a cathodic arc sputtering of a vanadium target in an oxygen atmosphere as described in our previous work. [36] The substrate was (001)-oriented Al_2O_3 and VO_2 (T) film thickness was about 80 nm.

An X-ray diffraction (XRD) pattern of the film in θ–2θ geometry was acquired using a Bruker AXS D8 DISCOVER setup with a Cu Kα (0.15418 nm) radiation.

Raman scattering study was done using a Horiba Jobin Yvon micro-Raman spectrometer LabRam HR800 with an x100 magnification objective (numerical aperture of 0.9). Measurements were conducted at room temperature in the air environment. A He-Ne laser with a 632.8 nm wavelength was used to excite Raman scattering. Laser power on the sample was 0.5 mW, and a spot diameter was about 2 μm. Raman mapping was done with a resolution of 2.5 μm. The spectra were collected in the range of 100–360 cm^{-1}. After subtracting the linear background, 8 pseudo-Voigt functions were used to fit the spectrum. The intensity of each Raman band was calculated as the area of the corresponding pseudo-Voigt peak. The total acquisition time for each point of the map was 2 min. All polarized measurements were done in the parallel (XX) configuration.

Scanning electron microscopy (SEM) images of VO_2 films were acquired using a Hitachi SU3500 SEM electron microscope operated at 20 kV. Additional higher resolution SEM images were obtained in a TM4000Plus microscope operated at 15 kV. In both cases, we used a backscattered electron detector since it provided the highest contrast for our samples.

Electron backscatter diffraction (EBSD) patterns were collected using a Hitachi SU3500 / Model3500 SEM electron microscope. The sample tilt was 70 °, and the distance between the sample and the detector was about 22 mm. The mapping was done with a resolution of 128 × 96 pixels on the area of 130 × 280 μm. Acquired maps were automatically analyzed by Bruker ESPRIT 2.1 software. For calculations, VO_2 (T) lattice constants and atomic positions were chosen according to ref [37].

3. Results and discussion

3.1. VO_2 (T) film overview

Vanadium oxide films consisting of micrometer-sized VO_2 (T) domains were investigated in detail in our previous work. [36] Briefly, the film contained two different regions: large flat crystalline domains (point I in Fig. 1a) and zones consisting of nanocrystalline grains (point II in Fig. 1a). Raman scattering (Fig. 1b) and X-ray diffraction (Fig. 1c) results demonstrated that the produced vanadium oxide phase is triclinic VO_2 (T). The crystals have two different orientations: (201) and (002). Detailed investigations revealed that (002) crystals are epitaxial, while (201) are not.

3.2. EBSD mapping

Crystal orientation in EBSD analysis is described in terms of three Euler angles (EA) (φ_1, φ, φ_2), where φ_1 is the first rotation is around Z, φ is the second rotation around X, and φ_2 is the third rotation around Z. Since VO_2 (T) phase can be described as a slightly distorted highly symmetric rutile structure, its automatic indexing using EA is ambiguous. Some examples are given in Fig. S1 (Supporting Information), where different crystal orientations correspond to nearly identical EBSD patterns. As a result, the EA map automatically generated by ESPRIT does not give any evidence about grain distribution [Fig. S2a (Supporting Information)]. We developed a simple algorithm to correct this (see Supporting Information for details). The resulting corrected map is shown in Fig. S2b (Supporting Information) and it was stretched and blended with SEM image (Fig. 2). Five different domains of VO_2 (T) (around points 1, 2, 3, 4 and 6) can be clearly seen. Sapphire substrate

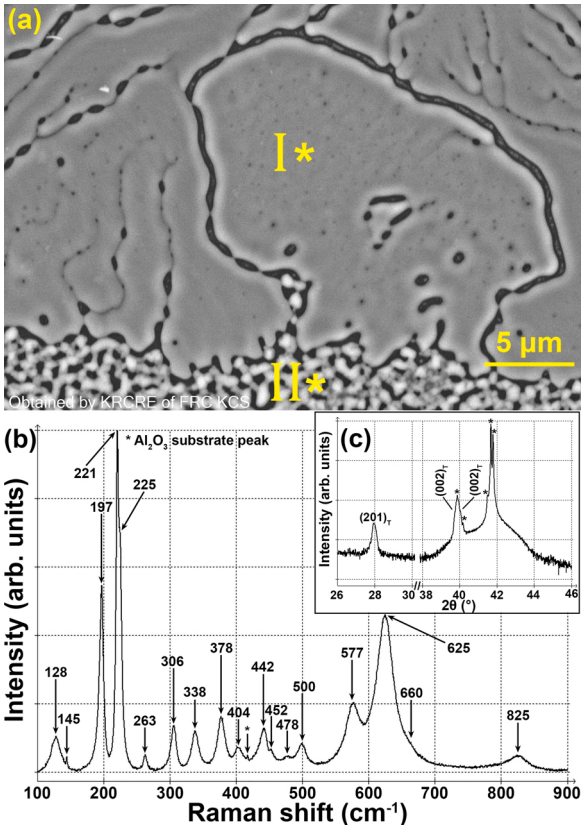

Fig. 1. (a) SEM image of the VO_2 (T) film. (b) Raman spectrum of a VO_2 (T) crystallite. (c) XRD pattern of the VO_2 (T) film (intensity is given in logarithmic scale).

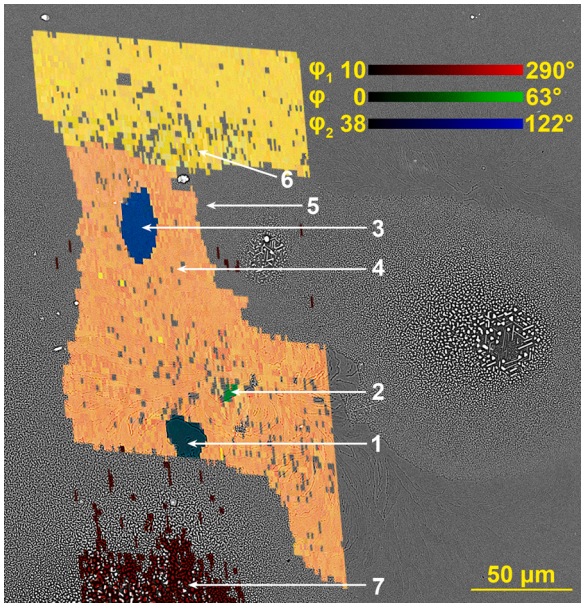

Fig. 2. EBSD map of VO_2 (T) film blended with SEM image. Red, green and blue channels are proportional to EA φ_1, φ and φ_2 respectively.

gives the dark red area at the bottom of the map (point 7). The area around point 5 does not give any good pattern due to the nanocrystalline character of the material.

For each domain, we chose the point with the best EBSD pattern and analyzed it manually. Since we expect only (201) and (002) orientations

of VO_2 (T), we tried to fit experimental patterns using simulations with EA of (φ_1, 45 °, 90 °) and (0, 0, φ_2) [or (0, 180 °, φ_2)]. The results are presented in Fig. 3 and Fig. S3 (Supporting Information) and summarized in Table 1. Three non-epitaxial (201) VO_2 (T) crystals (points 2, 4 and 6) and Al_2O_3 substrate (point 7) give very good agreement between experiment and simulation. On the other hand, the fit is not very good for epitaxial (002) VO_2 (T) crystals (points 1 and 3). It might be explained by the epitaxial stress or some out-of-plane misorientation of these domains.

3.3. Raman mapping

Raman map of the area similar to that shown in Fig. 2 was built based on intensities of Raman modes located around 222, 226, 309 and 340 cm^{-1} (Fig. 4). These particular modes were chosen to generate the false-color map since they are especially sensitive to crystallographic orientation highlighting the contrast between differently oriented crystallites. EBSD and Raman maps give similar pictures with a resolution of few μm. In contrast to EBSD mapping, Raman scattering gives a good signal from nanocrystalline VO_2 (T) areas (point 5). On the other hand, the Raman contrast between crystals 4 and 6 in Fig. 4 is faint.

To determine the orientation of VO_2 (T) at a certain point, additional Raman measurements involving full in-plane crystal rotations were applied. The intensity of each Raman mode depends on crystal orientation [36]:

$$I^{XX}_{A_{g(i)}(201)} \propto \left(\frac{1}{2}(a_i + c_i - 2d_i)\cos^2\psi + b_i\sin^2\psi + \frac{1}{\sqrt{2}}(e_i - f_i)\sin 2\psi\right)^2 \quad (1.1)$$

$$I^{XX}_{A_{g(i)}(002)} \propto \left(a_i\cos^2\psi + b_i\sin^2\psi + e_i\sin 2\psi\right)^2 \quad (1.2)$$

where a_i, b_i, c_i, d_i, e_i and f_i are Raman tensor elements for i-th mode and ψ is the third EA. Note that EA for Raman tensor formalism are determined as (φ, θ, ψ), where φ is the first rotation is around Z, θ is the second rotation around Y, and ψ is the third rotation around Z. Equations (1) were plotted in polar coordinates, where azimuth equals to ψ and radial vector equals to Raman mode intensity. Fig. 5 shows such plots for a few selected modes for three points of the map, while a complete set of data is presented in Fig. S4 (Supporting Information). Experimental curves are shifted relative to simulation depending on the initial orientation of the crystal in the spectrometer. This shift (dψ) is equal to the third EA and its average value for each crystal is given in Table 1. Fig. 5c and Fig. S4e (Supporting Information) show only experimental dependence with nearly constant intensities of all lines, which is consistent with nanocrystalline nature of the film at point 5.

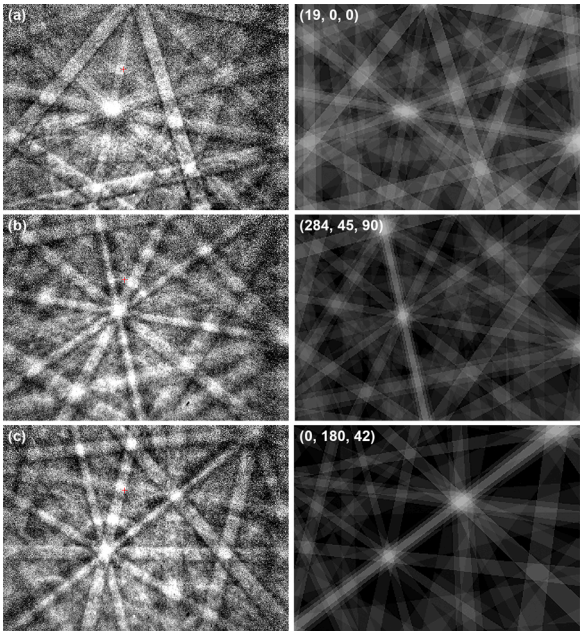

Fig. 3. Left: experimental EBSD patterns for points from Fig. 2: (a) 7 (Al_2O_3), (b) 4 and (c) 1. Right: simulated EBSD patterns for certain EA (φ_1, φ, φ_2).

Table 1
EA describing orientations of different VO_2 (T) crystals with respect to the Al_2O_3 substrate measured by EBSD (φ_1, φ, φ_2) and polarized Raman spectroscopy (φ, θ, ψ).

#	(φ_1, φ, φ_2)	(φ, θ, ψ)	$\alpha_{Raman} - \alpha_{EBSD}$
1 (002)	(0, 180, 42 °)	(0, 180 °, 74 °)	18°
2 (201)	(191 °, 45 °, 90 °)	(0 °, 45 °, 105 °)	–12°
3 (002)	(0, 0, 0 °)	(0, 0, –2 °)	16°
4 (201)	(284 °, 45 °, 90 °)	(0, 45 °, 7 °)	–7°
6 (201)	(274 °, 45 °, 90 °)	(0, 45 °, 7 °)	3°
7 (Al_2O_3)	(0, 0, 19 °)	–	–

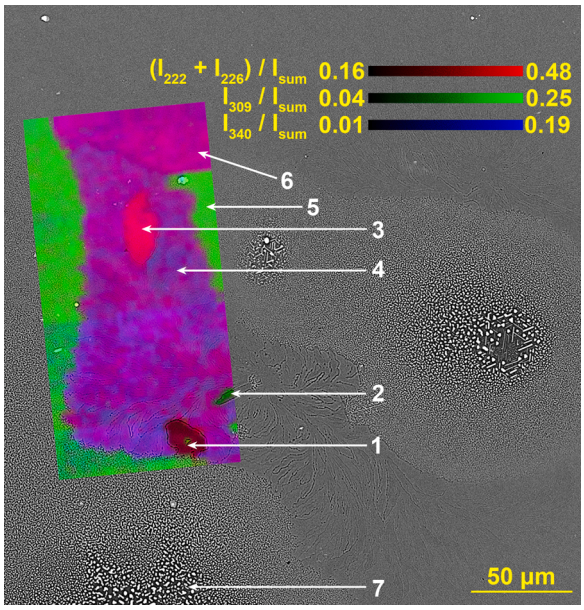

Fig. 4. Raman map of the VO_2 (T) film blended with SEM image. Red, green and blue channels are proportional to intensities of Raman lines (I_x is the intensity of the line near x cm^{-1}, I_{sum} is the integral intensity of the acquired spectrum).

The initial position of the sample in Raman spectrometer is shown in Fig. 6, and once we know dψ, we can determine the directions of lattice vectors. For both (002) and (201) crystals the angle between the laser beam polarization vector and the lattice vector ***b*** equals 90 ° – dψ.

To match the optical image (Fig. 6) with the electron image (Fig. 2 or 4) we have to apply a rotation by an angle of 81 °. So, the angle between the lattice vector ***b*** and horizontal axis in Fig. 2 can be calculated as $\alpha_{Raman} = 99° - \psi$.

Now we can compare this value with the results from EBSD measurements. EBSD map is slightly rotated with respect to Fig. 2 (by 5 °), so the angle between the lattice vector ***b*** and horizontal axis in Fig. 2 can be calculated as $\alpha_{EBSD} = 85° - \varphi_2$ for (002) crystal and $\alpha_{EBSD} = 85° - (270° - \varphi_1)$ for (201) crystal [since ($\varphi_1 = 270° - \alpha$, $\varphi = 45°$, $\varphi_2 = 90°$) is equivalent to ($\varphi = 0$, $\theta = 45°$, $\psi = \alpha$), where α is an arbitrary angle]. From Table 1 we can see a reasonably good agreement between crystal orientations determined by EBSD and polarized Raman measurements.

Triclinic VO_2 (T) may be considered as a continuously distorted variant of the VO_2 (M1) monoclinic phase and it exists at a wide range of lattice strains. [38] Our sample consists of many individual VO_2 (T) crystals and each of these crystals has its own structure with individual lattice constants and atomic positions. Experimentally, it was observed

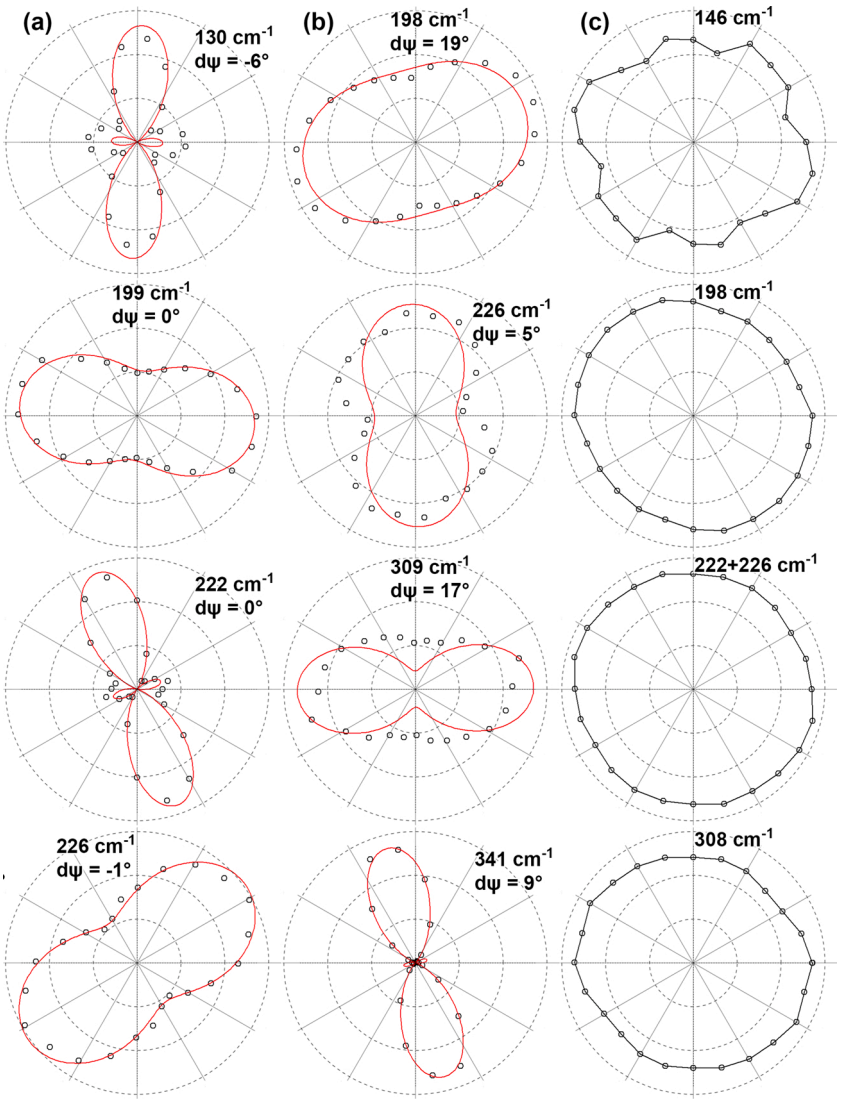

Fig. 5. Dependencies of Raman modes intensity on the sample rotation angle for points from Fig. 2: (a) 3, (b) 4 and (c) 5. The plots are given in polar coordinates. Theoretical fits based on equations (1) for (002) crystal (a) and (201) crystal (b) are given as solid red curves. Black open circles are experimental data after additional rotation by an angle of dψ.

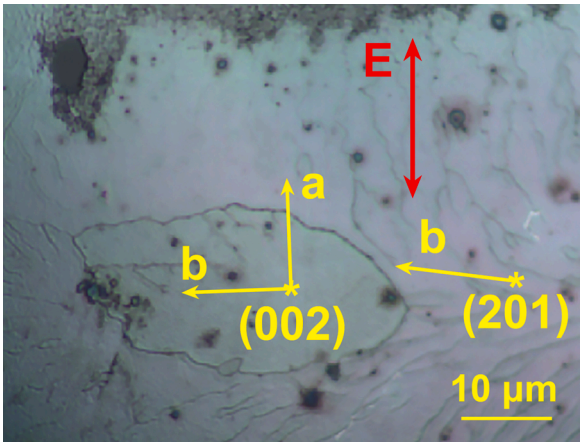

Fig. 6. Optical image of the area around points 3 and 4. Laser polarization is vertical. Lattice vectors are drawn based on Raman scattering measurements.

by XRD (the splitting of certain peaks into many narrow components) and by Raman spectroscopy (the shifting of certain peaks). [36] The variation of crystal structure leads to uncertainty in Raman tensor elements and although in most cases the deviation is not too significant, this is true not for all elements and all phonons. For instance, the fit for the mode at 309 cm^{-1} in Fig. 5b is made assuming $\frac{1}{2}(a+c-2d) = 58.5$, $b = 23$ and $\frac{1}{\sqrt{2}}(e-f) = 0.7$. The best fit will be achieved if we use the values of 54, 36 and 0.6, respectively. Thus, the value of b should be modified significantly, but the same behavior was observed for some elements in our previous work. [36] Also, if we apply the rotation of $d\psi = 7^\circ$ (the average angle for the crystal, instead of 17 °, the angle for the mode at 309 cm^{-1}), the coefficients to achieve the best fit will be 54, 37 and –2.5. Thus, the small variation of e and f tensor elements can cause significant angular uncertainty. This explains the misorientation on the order of ±15 ° observed in Table 1 and the large deviation of dψ for different lines of the same crystal.

Experimental dependencies of Raman mode intensity on sample rotation angle for crystal 1 can not be fitted by equation 1 using roughly the same values of dψ for all modes. During the measurements, we discovered that spectra for crystal 1 are similar to those for crystal 3 but they appear in the reverse order (as if the crystal is counterrotating)

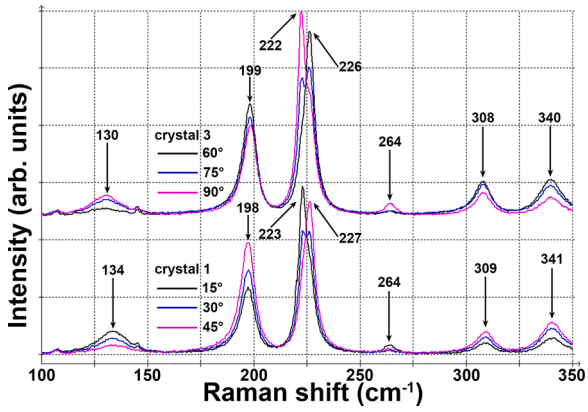

Fig. 7. Raman spectra for crystals 1 and 3 collected at different sample orientations.

(Fig. 7). It is possible if crystal 1 has EA θ = 180 °, i.e. lattice vector ***c*** is directed toward the substrate. Such crystal can be described by Eq. (1.2) if we assume the transformation of ψ → –ψ or, equivalently, $e_i \rightarrow -e_i$. The fact that we can determine θ for (002) crystal (θ = 0 or θ = 180 °) by Raman scattering results from the triclinic nature of our material. If we had monoclinic symmetry of VO_2 (M1), we would have $a_i = b_i = 0$ or $e_i = 0$. In both cases, I(ψ) = I(–ψ) and we would never observe the behavior similar to that shown in Fig. 7.

4. Conclusions

Triclinic vanadium dioxide films with micrometer-sized grains were mapped using EBSD and polarized Raman spectroscopy. Both methods could be used to distinguish differently oriented grains with a resolution of few μm. Euler angles determined by two different techniques showed relatively good agreement, verifying the results for VO_2 (T) Raman tensor element values obtained previously. We demonstrated that the triclinic nature of the sample could naturally remove the ambiguousness of some EA identification [θ = 0 or θ = 180 ° for (002) grains]. Overall, we show the capabilities of polarized Raman spectroscopy performed on the ordinary spectrometer on the real-life sample (crystals having varying lattice constants and epitaxial stress, the film morphology affected by the dewetting process). Our work is one of a few examples of polarized Raman investigation of crystals with the lowest (triclinic) symmetry.

Author statement

Petr Shvets: Methodology, Software, Formal analysis, Investigation, Writing - Original Draft

Alexander Shabanov: Investigation, Resources

Ksenia Maksimova: Conceptualization, Supervision, Writing - Review & Editing

Alexander Goikhman: Conceptualization, Project administration, Funding acquisition

Data availability

The data that support the findings of this study are available from the corresponding author upon reasonable request.

Declaration of Competing Interest

The authors declare that they have no known competing financial interests or personal relationships that could have appeared to influence the work reported in this paper.

Acknowledgements

This work was prepared with support from Ministry of Science and Higher Education of the Russian Federation (project FZWM-2020-0008).

The physicochemical analysis of materials (SEM and EBSD) was carried out in Krasnoyarsk Regional Center of Research Equipment of Federal Research Center "Krasnoyarsk Science Center SB RAS".

Appendix A. Supplementary data

Supplementary material related to this article can be found, in the online version, at doi:https://doi.org/10.1016/j.vibspec.2021.103328.

References

[1] J. De Gelder, K. De Gussem, P. Vandenabeele, L. Moens, J. Raman Spectrosc. 38 (2007) 1133, https://doi.org/10.1002/jrs.1734.
[2] A.C. Ferrari, J. Robertson, Phil. Trans. R. Soc. A. 362 (2004) 2477, https://doi.org/10.1098/rsta.2004.1452.
[3] T.P. Mernagh, A.G. Trudu, Chem. Geol. 103 (1993) 113, https://doi.org/10.1016/0009-2541(93)90295-T.
[4] M. Bouchard, D.C. Smith, Spectrochim. Acta A. 59 (2003) 2249, https://doi.org/10.1016/S1386-1425(03)00069-6.
[5] D.L.A. de Faria, S. Venâncio Silva, M.T. de Oliveira, J. Raman Spectrosc. 28 (1997) 873, https://doi.org/10.1002/(SICI)1097-4555(199711)28:11<873::AID-JRS177>3.0.CO;2-B.
[6] P. Shvets, O. Dikaya, K. Maksimova, A. Goikhman, J. Raman Spectrosc. 50 (2019) 1226, https://doi.org/10.1002/jrs.5616.
[7] S. Hanf, R. Keiner, D. Yan, J. Popp, T. Frosch, Anal. Chem. 86 (2014) 5278, https://doi.org/10.1021/ac404162w.
[8] R. Baddour-Hadjean, M.B. Smirnov, K.S. Smirnov, V.Yu Kazimirov, J.M. Gallardo-Amores, U. Amador, M.E. Arroyo-de Dompablo, J.P. Pereira-Ramos, Inorg. Chem. 51 (2012) 3194, https://doi.org/10.1021/ic202651b.
[9] G.D. Saraiva, J.G. da Silva Filho, A. Saraiva-Souza, A.J. Ramirode de Castro, A.M. R. Teixeira, C. Luz-Lima, F.G.S. Oliveira, V.O. Sousa Neto, P.T.C. Freire, F.F. de Sousa, Spectrochim. Acta A. 224 (2020), 117340, https://doi.org/10.1016/j.saa.2019.117340.
[10] L. Bayarjargal, C.-J. Fruhner, N. Schrodt, B. Winkler, Phys. Earth Planet. In. 281 (2018) 31, https://doi.org/10.1016/j.pepi.2018.05.002.
[11] R. Cuscó, E. Alarcón-Lladó, J. Ibáñez, L. Artús, J. Jiménez, B. Wang, M.J. Callahan, Phys. Rev. B 75 (2007), 165202, https://doi.org/10.1103/PhysRevB.75.165202.
[12] H.-N. Liu, X. Cong, M.L. Lin, P.-H. Tan, Carbon 152 (2019) 451, https://doi.org/10.1016/j.carbon.2019.05.016.
[13] P.S. Peercy, B. Morosin, Phys. Rev. B 7 (1973), https://doi.org/10.1103/PhysRevB.7.2779, 2779.
[14] Y. Kim, I.-H. Choi, J. Alloys. Compd. 770 (2019) 959, https://doi.org/10.1016/j.jallcom.2018.08.206.
[15] T. Mouri, M. Enami, J. Miner. Petrol. Sci. 103 (2008) 100–104, https://doi.org/10.2465/jmps.071015.
[16] P. Shvets, K. Maksimova, A. Goikhman, Physica B 613 (2021), 412995, https://doi.org/10.1016/j.physb.2021.412995.
[17] D. Bersani, S. Andò, P. Vignola, I.-G. Marino, P.P. Lottici, AIP Conf. Proc. 1163 (2009) 35–43, https://doi.org/10.1063/1.3222891.
[18] F.D. Hardcastle, I.E. Wachs, J. Phys. Chem. 95 (1991) 5031–5041, https://doi.org/10.1021/j100166a025.
[19] P. Mallet-Ladeira, P. Puech, C. Toulouse, M. Cazayous, N. Ratel-Ramond, P. Weisbecker, G.L. Vignoles, M. Monthioux, Carbon 80 (2014) 629, https://doi.org/10.1016/j.carbon.2014.09.006.
[20] R.L. Frost, W.N. Martens, L. Rintoul, E. Mahmutagic, J.T. Kloprogge, J. Raman Spectrosc. 33 (2002) 252, https://doi.org/10.1002/jrs.848.
[21] J.T. Kloprogge, R.L. Frost, L. Rintoul, Am. Miner. 89 (2004) 352, https://doi.org/10.2138/am-2004-2-314.
[22] R. Loudon, Adv. Phys. 13 (1964) 423, https://doi.org/10.1080/00018736400101051.
[23] M. Deluca, M. Higashino, G. Pezzotti, Appl. Phys. Lett. 91 (2007), 091906, https://doi.org/10.1063/1.2776357.
[24] S. Kim, J. Lee, C. Lee, S. Ryu, J. Phys. Chem. C 125 (2021) 2691, https://doi.org/10.1021/acs.jpcc.0c09938.
[25] Y. Zhu, W. Zheng, W. Wang, S. Zhu, L. Li, L. Cheng, M. Jin, Y. Ding, F. Huang, PhotoniX 1 17 (2020), https://doi.org/10.1186/s43074-020-00017-7.
[26] M.-L. Lin, Y.-C. Leng, X. Cong, D. Meng, J. Wang, X.-L. Li, B. Yu, X.-L. Liu, X.-F. Yu, P.-H. Tan, Sci. Bull. 65 (2020) 1894, https://doi.org/10.1016/j.scib.2020.08.008.
[27] X. Xu, Q. Song, H. Wang, P. Li, K. Zhang, Y. Wang, K. Yuan, Z. Yang, Y. Ye, L. Dai, ACS Appl. Mater. Interfaces 9 (2017) 12601, https://doi.org/10.1021/acsami.7b00782.
[28] D. Yoon, H. Moon, Y.-W. Son, G. Samsonidze, B.H. Park, J.B. Kim, Y.P. Lee, H. Cheong, Nano Lett. 8 (2008) 4270, https://doi.org/10.1021/nl8017498.
[29] W. Zheng, R. Zheng, F. Huang, H. Wu, F. Li, Photonics Res. 3 (2015) 38, https://doi.org/10.1364/PRJ.3.000038.
[30] M. Zaghrioui, J. Sakai, N.H. Azhan, K. Su, K. Okimura, Vib. Spectrosc. 80 (2015) 79, https://doi.org/10.1016/j.vibspec.2015.08.003.

[31] M. Tsuboi, J.M. Benevides, G.J. Thomas, Proc. Jpn. Acad., Ser. B, Phys. Biol. Sci. 85 (2009) 83, https://doi.org/10.2183/pjab/85.83.
[32] O. Ilchenko, Y. Pilgun, A. Kutsyk, F. Bachmann, R. Slipets, M. Todeschini, P. O. Okeyo, H.F. Poulsen, A. Boisen, Nat. Commun. 10 (2019) 5555, https://doi.org/10.1038/s41467-019-13504-8.
[33] F.J. Morin, Phys. Rev. Lett. 3 (1959) 34, https://doi.org/10.1103/PhysRevLett.3.34.
[34] Z. Shao, X. Cao, H. Luo, P. Jin, NPG Asia Mater. 10 (2018) 581, https://doi.org/10.1038/s41427-018-0061-2.
[35] A. Bailly, S. Grenier, M.M. Villamayor, M. Gaudin, A.Y. Ramos, P. Bouvier, C. Bouchard, L. Magaud, L. Laversenne, B. Mongellaz, E. Bellet-Amalric, A. Lacoste, A. Bès, J. Appl. Phys. 126 (2019), 165306, https://doi.org/10.1063/1.5113771.
[36] P. Shvets, K. Maksimova, A. Goikhman, J. Appl. Phys. 129 (2021), 055302, https://doi.org/10.1063/5.0032916.
[37] M. Ghedira, H. Vincent, M. Marezio, J.C. Launay, J. Solid State Chem. 22 (1977) 423, https://doi.org/10.1016/0022-4596(77)90020-2.
[38] J.M. Atkin, S. Berweger, E.K. Chavez, M.B. Raschke, Phys. Rev. B 85 (2012), 020101, https://doi.org/10.1103/PhysRevB.85.020101.